

Flow pattern in the scour hole around a cylinder

Écoulement dans une fosse autour d'un cylindre

W.H. GRAF and I. ISTIARTO, *Laboratoire de recherches hydrauliques, École Polytechnique Fédérale, CH-1015 Lausanne, Switzerland*

ABSTRACT

Local scour around a bridge pier (cylinder) is a problem of much concern to hydraulic engineers. This is a complex phenomenon resulting from the interaction of the three-dimensional turbulent flow field around the cylinder and the mobile channel bed (see Fig. 1). In the vicinity of the cylinder, scouring is the consequence.

In this paper, the three-dimensional flow field in an established (equilibrium) scour hole is experimentally investigated. An acoustic-Doppler velocity-profiler (ADVP) was used to measure instantaneously the three components of the velocities in the vertical symmetry (stagnation) plane of the flow before and after the cylinder. The vorticity of the flow field was calculated. Results of the study show, that a vortex-system is established in the front and a trailing wake-vortex system of strong turbulence is formed in the rear of the cylinder.

RÉSUMÉ

L'érosion locale autour d'un cylindre est un problème auquel les hydrauliciens sont souvent confrontés. C'est un phénomène complexe qui est à l'origine de l'interaction de l'écoulement tridimensionnel turbulent autour du cylindre et le fond mobile du canal (voir Fig. 1). L'érosion autour du cylindre est une conséquence directe de cette interaction.

Dans cet article, on présente les résultats d'une étude expérimentale de l'écoulement tridimensionnel dans la fosse d'érosion autour du cylindre. Le champ de vitesse ainsi que celui de la vorticit  en amont et en aval du cylindre sont d crits   partir de mesures des trois composantes de vitesse instantan e. Un profileur v locim trique acoustique Doppler est utilis  pour effectuer les mesures. L'analyse des r sultats montre l' tablissement d'un tourbillon   l'amont du cylindre et d'un sillage fortement turbulent derri re le cylindre.

Introduction

Unidirectional flow in a mobile channel which encounters a protruding vertical obstacle, becomes three-dimensional. The resulting flow pattern around a cylinder becomes complex and is difficult to assess hydrodynamically. Upon reaching a certain flow velocity in the channel, the sediment particles close to the cylinder begin to move; scour is initiated. The eroded particles will follow the flow pattern and are carried from the front of the cylinder towards the downstream. Upon an increase in the flow velocity, more and more particles will get dislodged, forming a *scour hole* increasing in size and depth. Eventually a maximum (equilibrium) scour depth is attained, which corresponds to a flow velocity being close to the critical velocity for initiation of sediment transport in the channel. For non-uniform sediments, the larger grain are less likely to be eroded and an armoring layer forms itself in the scour hole.

Scour is initiated at, or close to, the nose of the cylinder. The scour hole grows in depth and in volume by forming a groove. The upstream portion of the scour hole has the approximate shape of an inverted cone-like surface, stretching around the cylinder with side slopes about equal to the angle of repose of the sediments. Eroded material is transported – often in forms of bursts – towards the rear of the cylinder, where it may or may not be deposited. The maximum scour depth for a cylindrical object is in general located in front of the object (see Fig. 1).

Results of various studies (see Shen, 1971, p. 23/4; Melville, 1975; Raudkivi, 1991, p. 62; and Graf and Altinakar, 1998, Ch. 9) have shown that different components of the flow pattern might play a role in local scouring (see Fig. 1).

Flow in a channel, being a boundary-layer flow, $u(z)$, approaches the cylinder and a stagnation pressure, $p_s(z)$, decreasing with depth, establishes itself. This will produce a (weak) pressure gradient along the front of the cylinder and induce a *downward flow*. Since there is also a pressure gradient around the cylinder, $p(\alpha)$, the downstream flow will be laterally diverted. Due to the stagnation pressure in front of the cylinder, the water surface increases, forming a *bow wave*. If the pressure increase becomes sufficiently strong, the three-dimensional boundary layer undergoes separation and rolls up ahead of the cylinder. A *horseshoe-vortex system* forms at the base of the cylinder. This vortex stretches into the downstream direction, diminishing its strength, and is active in the local scour process. A trailing *wake-vortex system* is formed

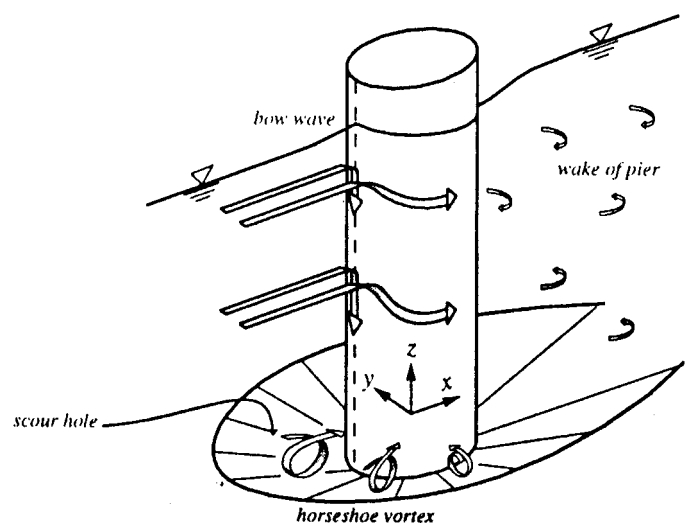


Fig. 1 Schema of flow pattern and local scour around a cylinder.

Revision received February 28, 2001. Open for discussion till August 31, 2002.

in the rear of the cylinder over the entire flow depth. There the turbulence intensity is increased and consequently erosion and transport of sediments is enhanced.

This study investigates experimentally the flow pattern in the vertical symmetry (stagnation) plane in the established (equilibrium) scour hole in front and rear of the cylinder positioned vertically on a mobile channel bed. It is an extension of the study of flow around a cylinder on a horizontal and fixed (non-mobile) bed performed by Graf and Yulistiyanto (1998).

Installation and measuring equipment

The experiments were conducted in a 29 [m] long and 2.45 [m] wide rectangular channel having a uniform sand bed of mean diameter $d_{50}=2.1$ [mm]. The cylinder with a diameter of $D_p = 15$ [cm], was vertically installed at $x_L = 11$ [m] downstream of the channel entrance. The uniform approach flow ($Q = 0.2$ [m³/s], $U_\infty = 0.45$ [m/s] and $h_\infty = 18$ [cm]) was established and can be considered to be two-dimensional ($B/h_\infty = 13.6$), turbulent ($Re = 81,000$), and subcritical ($Fr = 0.34$). The shear velocity was obtained from the measured velocity and shear-stress distributions, as being $u_{*,\infty} = 2.65$ [cm/s]. The velocity measurements were performed in the equilibrium scour hole ($d_s = 25$ [cm]) under clear-water scour condition which had been previously established by performing a continuous run of 5 to 7 days.

An acoustic Doppler velocity profiler (ADVP), developed at the *Laboratoire de recherches hydrauliques* (see Lhermitte and Lemmin, 1994; Hurther and Lemmin, 2001), was used to measure the instantaneous velocity vector. This non-intrusive instrument measures instantaneously three-dimensional velocities at a number of layers – in 0.3 or 0.5 [cm] intervals – within a water column based on the backscattered acoustic signals. The acoustic emitter of the ADVP and its 4 receivers were placed in a water-filled housing above the water surface which slightly penetrated the flow. A Mylar film provides the interface between the housing and the water surface; the flow perturbation is thus minimized (see Figs. 4 and 5). The velocity profile was obtained by recording the backscattered signals coming from the layers within the water column. A time gating procedure was applied to group the signals coming from different layers, which allows the discrete vertical positioning of each data point. This defines also the thickness of the measuring volume, Δh , to be calculated from the relation $\Delta h = \Delta T \cdot c_s / 2$, where $\Delta T = 4$ or 6 [μ s] is the time gate and $c_s = 1486$ [m/s] the acoustic speed in water. The diameter of the measuring volume, $\Delta\phi$, is given by the size of the conical acoustic beam, being for the two types of the emitter used, $6 \leq \Delta\phi$ [mm] ≤ 26 . It is assumed that homogeneous turbulence prevails within the measuring volume. The signal recording was typically done at 667 [Hz] or 910 [Hz]. Each instantaneous velocity is obtained from 32 signal time-series, resulting in a measuring frequency of 20 [Hz] or 28 [Hz]. A 60 [s] duration was typically done to get one velocity profile.

Vertical distributions of the velocity, of the turbulence intensity, and of the Reynolds stress were obtained at 26 positions in front of the cylinder and at 16 positions at the rear side. For technical

reasons, the measurements within the scour-hole region were performed in two separate series, i.e. those close to the water surface and those underneath up to the bed. A nearly perfect overlapping of the two data sets is observed for the measurements in front of the cylinder, while for those at the rear of the cylinder, it is not completely so. The ADVP-instrument was installed in a way that measurements in some regions could not be obtained, i.e. in the upper part and close to the cylinder ($z > 5$ [cm] within $-20 < x$ [cm] < 22), at the immediate vicinity (2.5 [cm]) from the cylinder and close (2 [cm]) to the water surface (see Figs. 4 and 5).

Measurements in the plane upstream of cylinder

The scour hole in the upstream plane of the cylinder ($\alpha = 0^\circ$) starts at $x \approx -45$ [cm] ($-3 D_p$), reaching the maximum scour depth of $d_s = 25$ [cm] ($1.67h_\infty$) at the leading edge of the cylinder; the downward incline into the scour-hole is thus $\theta = 35^\circ$. At 25 positions the vertical distributions of velocities, of Reynolds stresses, and of turbulence intensities are obtained from the ADVP measurements. The data are taken over a distance of $-80 \leq x$ [cm] ≤ -10 , which cover the approach-flow region outside the scour hole and the scour-hole region. For $x \leq -20$ [cm], the data cover almost the entire flow depth, while for $x > -20$ [cm], the data are only available at $z \leq 5$ [cm] (see Fig. 4). While all 25 distributions are used for evaluation (see Istiarto, 2001), here only the distributions at 7 measuring positions, being rather representative ones, will be presented (see Fig. 2).

The measured vertical distributions of the time-averaged longitudinal, $u(z)$, and vertical, $w(z)$, velocity components in the $\alpha = 0^\circ$ plane are shown in Fig. 2, while in Fig. 4 is given the velocity-vector, (u, w), distribution.

- Approaching the cylinder the u -component diminishes over the entire depth, beginning at $x > -20$ [cm] to show negative values, notably close to the bed.
- In the approach region, $x \leq -42$ [cm], the w -component remains negligible, but subsequently grows considerably and reaches important negative (downward) values of $w \approx -0.27$ [m/s] ($-0.6U_\infty$), notably in the lower part, $z \leq 0$, and close to the cylinder, which is in agreement with data reported by Raudkivi (1998, p. 248).
- The v -component (not shown here) remains practically negligible, but shows in the lower part, $z \leq -9$ [cm], and close to the cylinder, small values of $v \approx -0.03$ [m/s], indicating that the flow becomes three-dimensional.

The flow pattern (see Fig. 4) is such that at the start of the scour hole the flow separates, $\theta_s > 6^\circ$ (see Schlichting, 1979, p.628), subsequently showing a weak clockwise vorticity. At the cylinder an adverse pressure gradient creates a downward flow being returned at the bottom of the scour hole – showing a strong clockwise vortex, usually referred to as horseshoe vortex. Similar observations have been reported in the literature (see Shen et al., 1963; Melville and Raudkivi, 1977; Dey et al., 1995; Kobayashi et al., 1997 and Ahmed and Rajaratnam, 1998).

Reasonably successful numerical simulations of the flow pattern have been recently proposed (see Richardson and Panchang,

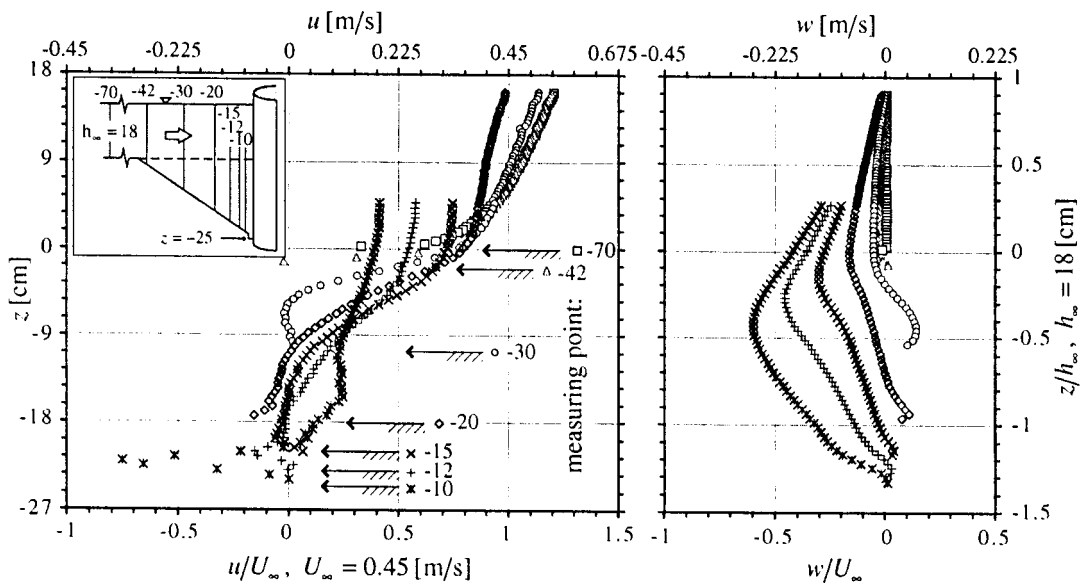


Fig. 2 Measured velocities in the plane upstream of cylinder.

1998; Istiarto, 2001).

The data of the velocity fields (see Figs. 2 and 4) can readily be used to generate the vorticity contours; this is shown in Fig. 6, where only the region of significant vorticity, $z \leq 2$ [cm], is displayed. The clockwise positive vorticity was defined as:

$$\omega_y = \frac{\partial u}{\partial z} - \frac{\partial w}{\partial x} \quad (1)$$

it was calculated from the respective velocity components – data from all 25 measuring positions are evaluated – using a centre finite-difference scheme. The following is to be observed:

- Due to a change in the incline of the bottom, a positive vorticity is strong at the brink, subsequently at $x \approx -35$ [cm], a weak counter-clockwise vorticity is noticed.
- In the downstream part of the scour hole – directly upstream of

the cylinder –, caused by the adverse pressure gradient due to the flow obstruction of the cylinder, a rather strong clockwise vortex is situated at $x \approx -10$ [cm].

- In the remaining part of the scour-hole the (positive) vorticity is rather weak, being of the same order as the vorticity in the approach flow.

Similar observations are reported by Kobayashi et al. (1997). Estimation of the bed shear-stress, τ_b , from the experimental data is a rather difficult task. While a direct measurement technique would be most desirable, here we must content ourselves with the available data from the velocity and shear-stress distributions (see Fig. 4 and Fig. 9). Three alternative methods were used:

- i) based on the velocities, u and w , measured closest to the bed, $z \approx 4$ [mm], a velocity parallel to the bed – at a distance of n – was calculated, V_{par} ; the bed shear-stress was subsequently computed as:

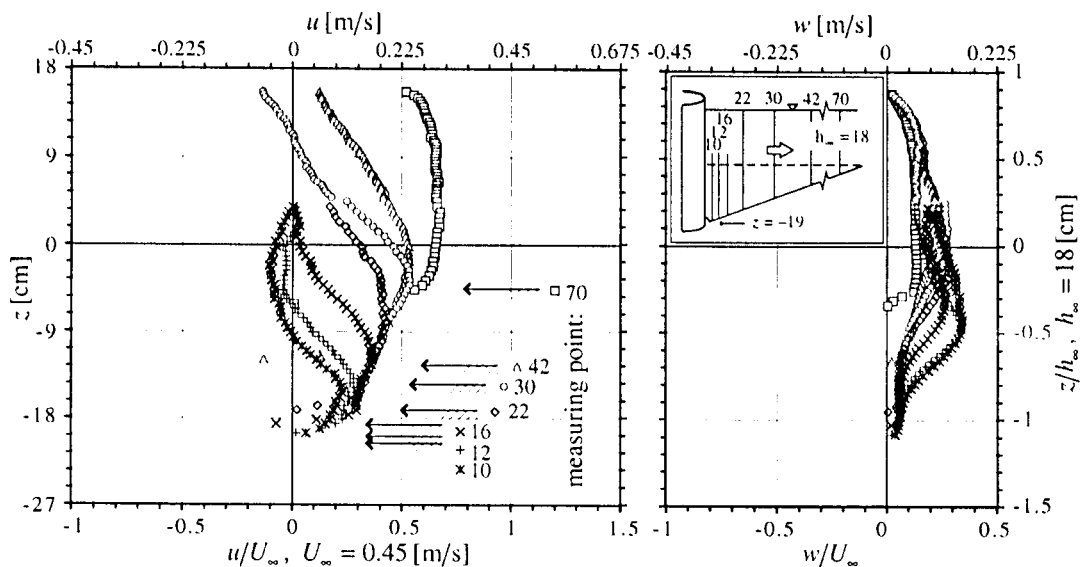


Fig. 3 Measured velocities in the plane downstream of cylinder.

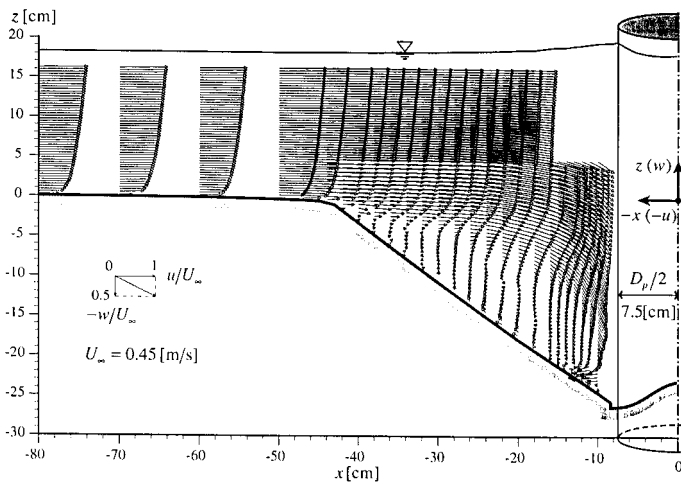


Fig. 4 Measured velocity field in the plane upstream of cylinder.

$$\tau_{o,1} = \rho v_t \left(\frac{\partial V_{par}}{\partial n} \right) \quad (2)$$

where $v_t = 1.3 \times 10^{-5} \text{ [m}^2/\text{s}^2]$ was taken as the measured eddy viscosity in the approach flow. A rather similar method was used by Melville and Raudkivi (1977).

- ii) based on the measured shear-stress distribution (see Fig. 9) a (rather subjective) extrapolation towards the bed was used to obtain the bed shear-stress, or:

$$\tau_{o,2} = -\rho (\overline{u'w'}) \Big|_{bed} \cos \theta \quad (3)$$

based on a relation for the velocity distribution (see Graf and Altinakar, 1998, Eq. 3.20) the bed shear-stress was evaluated by:

$$\tau_{o,3} = \rho (u_{*3})^2 = \rho \left(U \sqrt{\frac{g}{C^2}} \right)^2 = \rho (0.07 U)^2 \quad (4)$$

where U is the local depth-averaged flow velocity and C is the Chézy coefficient taken as $C = 44 \text{ [m}^{1/2}/\text{s}]$.

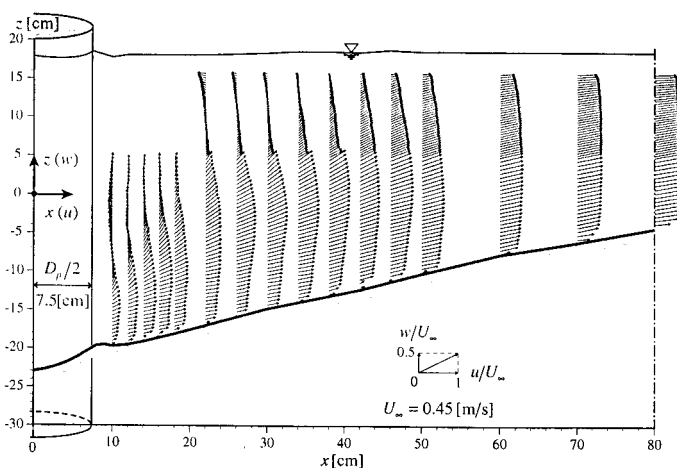


Fig. 5 Measured velocity field in the plane downstream of cylinder.

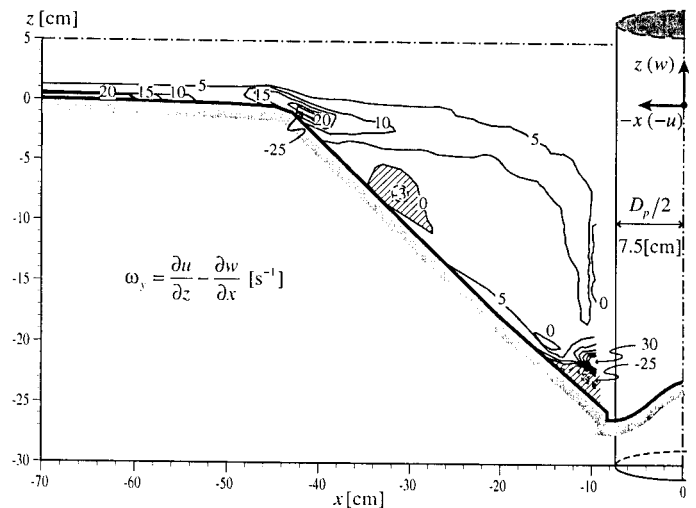


Fig. 6 Vorticity field in the plane upstream of cylinder.

The mean bed shear-stress, τ_o , obtained by these three methods is presented in Fig. 8 and the following is to be remarked:

- In the approach region, $x \leq -45 \text{ [cm]}$, all three methods render rather similar results, being $0.6 \leq \tau_o \text{ [Pa]} \leq 1.0$. The bed shear-stress in the approach region was earlier obtained as being $\tau_{o\infty} = 0.70 \text{ [Pa]}$ or $u_{*c\infty} = 2.65 \text{ [cm/s]}$.
- In the region of the scour hole, $x \geq -45 \text{ [cm]}$, the agreement is less convincing. It appears to us that the data using the velocity measurements, Eq.2, seem to be more reliable; evaluation of the measurement of the velocity, V_{par} , is more objective than the one of the shear-stress, $-\rho (\overline{u'w'})$, at the bed. The global method, Eq.4, would be simple, but applies essentially to uniform flow and does not take into account the flow reversal close to the bed, thus the sign change is not respected. Note, that the negative value indicates flow reversal at the bed.
- In both regions the critical shear-stress, $\tau_{o,cr} = 1.36 \text{ [Pa]}$, as calculated from the Shields diagram, $\tau_{cr}^* = 0.04 \text{ [-]}$, was not exceeded. This is in agreement with eye observations. Thus our experiment is well a clear-water scour run, where the capacity of transport out of the scour hole is zero.

The (high) bed shear-stress in the approach flow is gradually re-

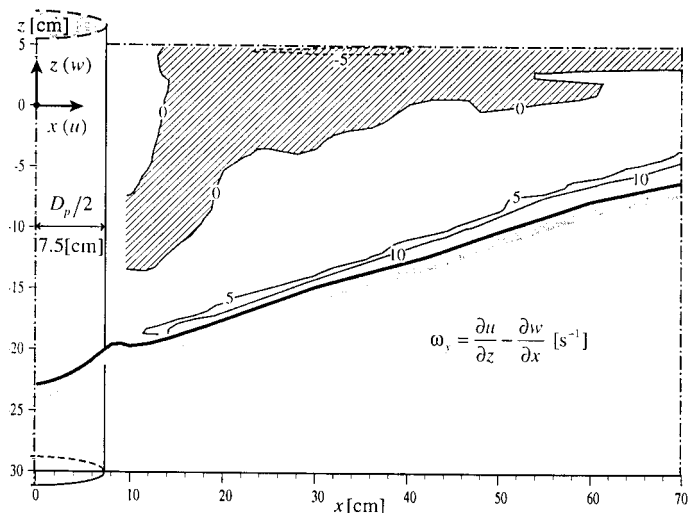


Fig. 7 Vorticity field in the plane downstream of cylinder.

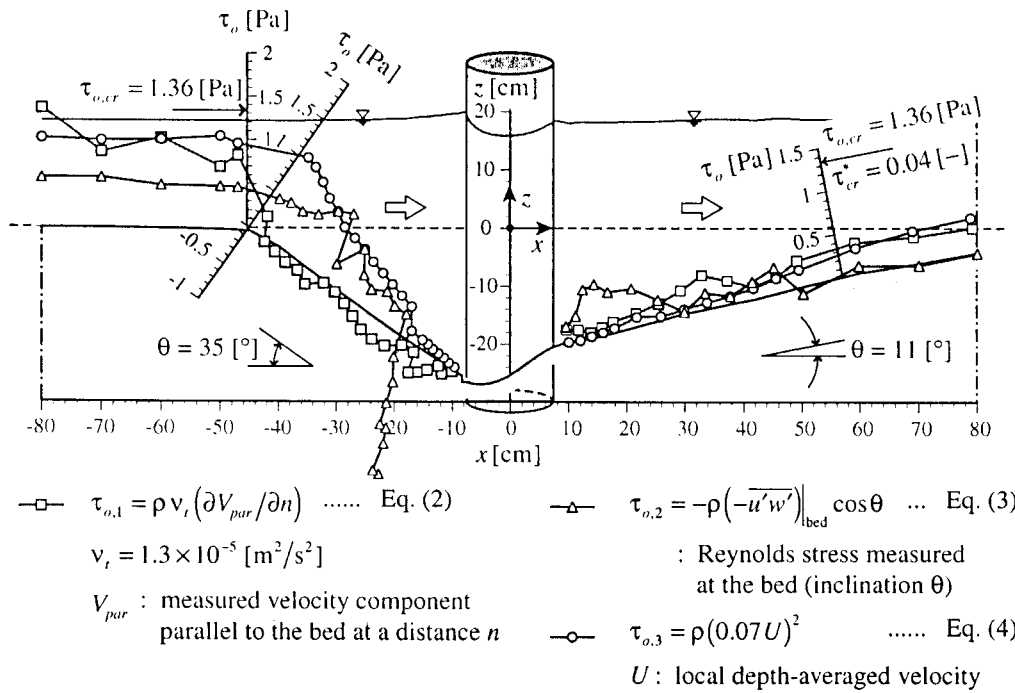


Fig. 8 Estimated bed-shear stress in the plane upstream and downstream of cylinder.

duced on entering the scour hole, where the shear stress remains rather low on approaching the cylinder. Measurements by Melville and Raudkivi (1977, p. 379) show a rather similar trend. The results obtained from the turbulence measurements are shown in Fig. 9, where $u_{*∞}$ is the shear velocity in the approach flow, $U_∞$. Also plotted (see Fig. 11) is the distribution of the turbulent kinetic energy of the flow, defined as:

$$k = \frac{1}{2} (\overline{u'u'} + \overline{v'v'} + \overline{w'w'}) \quad (5)$$

The following is to be observed:

- the longitudinal turbulence intensities, $\sqrt{\overline{u'u'}}$, are the dominant ones and this over the entire flow depth,

- outside the scour hole, $z > 0$, the profiles of the turbulence intensities, $\sqrt{\overline{u'u'}}$, $\sqrt{\overline{v'v'}}$, and $\sqrt{\overline{w'w'}}$, reasonably collapse,
- on entering the scour hole, where flow separation occurs, at what appears to be the zone of flow separation, there is to be seen a pronounced bulge in the turbulent energy, k , profile which bends downwards,
- on approaching the cylinder, where downflow occurs, the turbulent energy, k , becomes increasingly strong, notably at the foot of the cylinder, where the clockwise turning vortex is placed (see Fig. 6),
- the Reynolds stress, $-\overline{u'w'}$, remains reasonably linear in the upper part, $z > 0$, and shows distinguishable bulges in the lower part, $z < 0$, moving downstream and downwards towards the foot of the cylinder.

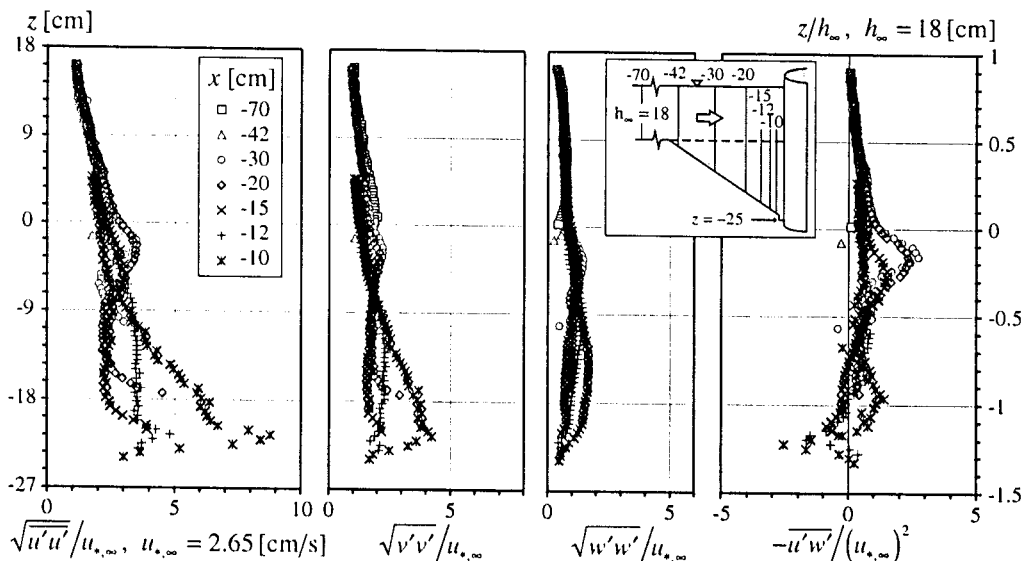


Fig. 9 Measured turbulence intensities and shear-stresses in the plane upstream of cylinder.

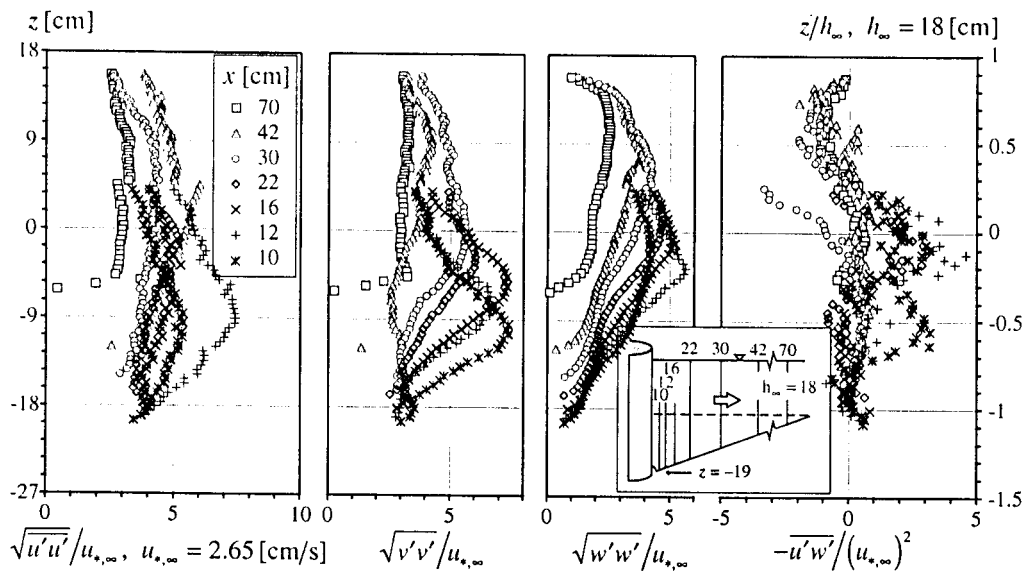


Fig. 10 Measured turbulence intensities and shear-stresses in the plane downstream of cylinder.

Unfortunately – to the best of our knowledge – no research is available for comparison. Studying a backward-facing step, Etheridge and Kemp (1978, p. 555) and Nakagawa and Nezu (1987, p. 70) showed rather similar trends.

Measurements in the plane downstream of the cylinder

The scour hole in the plane downstream of the cylinder ($\alpha = 180^\circ$) extends far towards the downstream, $x = 105$ [cm] ($7D_p$), with the maximum scour depth of $d_s = 19$ [cm] ($1.3h_{sc}$); the upward incline of the scour hole is thus $\theta = 11^\circ$. Further downstream, up to $x = 300$ [cm] ($20D_p$), the bed continues with a deposition. The ADVP measurements were performed at $10 \leq x$ [cm] ≤ 100 , where 18 vertical distributions of the velocities, Reynolds stresses and turbulence intensities were obtained (Istiarto, 2001). The data for the region close to the cylinder, $x < 22$ [cm], are available only at $z \leq 5$ [cm], while those for the rest, $x \geq 22$ [cm], cover almost the entire flow depth.

The measured vertical distributions of the time-averaged longitudinal, $u(z)$, and vertical, $w(z)$, velocity components are shown in Fig. 3, where only those at 7 measuring positions, being rather

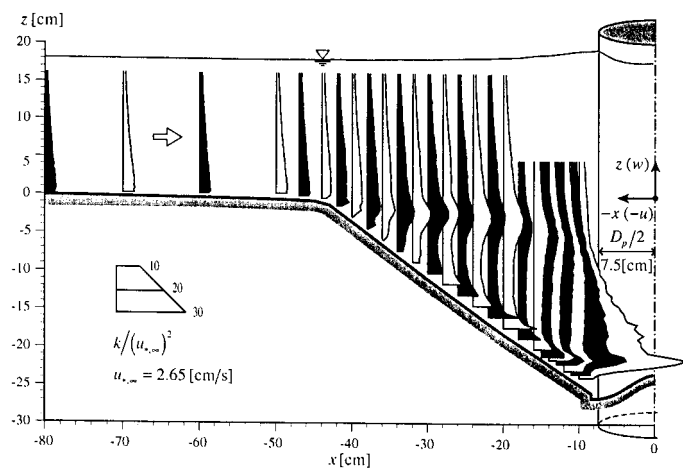


Fig. 11 Turbulent kinetic energy in the plane upstream of cylinder.

representative ones, are presented. Given in Fig. 5 is the distribution of the velocity vector, (u, w) ; presented here are 16 distributions in the range of $10 \leq x$ [cm] ≤ 80 .

- Close and behind the cylinder the u -components are small and show clearly flow reversal towards the water surface. Moving outwards from the scour hole the u -components increase and flow reversal diminishes. Flow is almost back to a logarithmic one at $x \approx 100$ [cm].
- The w -components have always positive (upwards) values, being behind the cylinder large, $w \approx 0.16$ [m/s], and diminishing as the flow leaves the scour hole.
- The v -components (not shown here) are usually very small. However, immediately after the cylinder they reach larger values of $v \approx 0.04$ [m/s], again an indication of weak three-dimensional flow.

The flow patterns (see Fig. 5) show clearly the flow reversal of a weak counter-clockwise vortex, diminishing towards the downstream. Similar observations have been reported in the literature (see Melville and Raudkivi, 1977, and Dey et al., 1995).

The vorticity contours – using the definition given with Eq. 1 – are shown in Fig. 7.

- Positive vorticity is probably due to the boundary-layer flow in the vicinity of the scoured bed.
- Very weak negative vorticity is evident in the upper layers, resulting in the weak counter-clockwise vortex, which disappears when the flow moves out of the scour hole.

The mean shear stress, τ_o , obtained with the different methods, outlined above, is presented in Fig. 8. The following is to be remarked:

- In the region of the scour hole, $10 \leq x$ [cm] ≤ 80 , the three methods render surprisingly similar results, being $0 \leq \tau_o$ [Pa] ≤ 0.5 , thus almost constant over the entire length measured. The measured bed shear-stress is slightly larger than the one in the upstream part of the scour hole; this was also observed by Melville and Raudkivi (1977, p. 379) and Dey (1997, p. 33).
- The critical shear-stress, $\tau_{o,cr} = 1.36$ [Pa], is never reached;

clear-water scour, also observed by eye, is maintained.

- The shear stress on leaving the scour has about the same (absolute) value as the one in the upstream part of the scour hole; there is a weak tendency of an increase as leaving the scour hole.

The results obtained from the turbulence measurements are shown in Fig. 10; also plotted (see Fig. 12) is the distribution of the turbulent kinetic energy, Eq.1. The following can be observed:

- Behind the cylinder and up to $x \approx 70$ [cm] the turbulence is rather isotropic and strong; flow in the wake is known to be 3-D flow.
- Only when leaving the scour hole, $x > 70$ [cm], does the turbulence profile return to the situation of the approach flow.
- The turbulent energy, k , shows a typical bulge above the bed of the scour hole, which diminishes going downstream.
- The intensity of the turbulence behind the cylinder is stronger than upstream of the cylinder.
- The Reynolds-stress distribution shows a rather chaotic picture.

Conclusions

The results of an experimental study of the flow pattern in the upstream and downstream plane of a cylinder, positioned vertically in the scour hole, are presented. Detailed measurements were obtained with a non-intrusive instrument (ADVP), which measured the instantaneous velocity vectors in the approach and scour-hole.

In the upstream reach of the cylinder a vortex system was detected, being a rather strong one, known as the horseshoe vortex, positioned at the foot of the cylinder. Another but weaker vortex (not so visible) is probably due to the change in the slope of the bottom leading into the scour hole.

In the downstream reach of the cylinder there exists a flow reversal towards the water surface. This is rather pronounced immediately after the cylinder, but gradually returns to a logarithmic profile further downstream. The vorticity in this region is rather weak.

The longitudinal distribution of the bed shear-stress shows that the shear stress is considerably reduced in the scour hole when

compared to its value in the approach flow. The bed shear-stress has opposite sign in the upstream and downstream part of the scour hole. Throughout the measurements the bed shear-stress is always smaller than the critical one.

The distributions of the turbulence intensity as well as of the Reynolds stress were evaluated. The turbulent kinetic energy is very strong at the foot of the cylinder on the upstream side; it is also very strong in the wake behind the cylinder.

Acknowledgements

The second author would like to thank the Swiss Federal Commission on Scholarships for Foreign Students for providing him with the financial support during the early phase of the research. The use of the ADVP instrument was greatly facilitated by the help of D. Hurther and U. Lemmin. The fruitful discussions with M.S. Altınakar and Y. Zech during the entire study are highly appreciated.

Notations

B	channel width [L].
C	Chézy coefficient [$L^{1/2}/T$].
D_p	diameter of cylinder [L].
d_{50}	mean diameter of sediment [L].
d_s	equilibrium scour depth [L].
Fr	Froude number, $Fr = U_\infty \sqrt{g h_\infty}$ [-].
g	gravitational acceleration [L/T^2].
h	flow depth [L].
k	turbulent kinetic energy, $k = \frac{1}{2} (\overline{u'u'} + \overline{v'v'} + \overline{w'w'})$ [L^2/T^2].
n	normal distance from the bed [L].
Q	discharge [L^3/T].
Re	Reynolds number, $Re = U_\infty h_\infty / \nu$ [-].
U	depth-averaged velocity [L/T].
u_*	shear velocity [L/T].
u, v, w	cartesian velocity components in the $x, y,$ and z directions, respectively [L/T].
u', v', w'	fluctuating velocity components [L/T].
V_{par}	velocity parallel to the bed [L/T].
x, y, z	cartesian coordinate in the longitudinal, transverse, and vertical directions, respectively [L].
α	angular direction [$^\circ$].
θ	bed slope of the scour hole [$^\circ$].
ν	kinematic viscosity of water [L^2/T^2].
ν_t	turbulent eddy viscosity [L^2/T^2].
ρ	density of water [M/L^3].
τ_o	bed shear-stress [$M/L/T^2$].
$\tau_{o,cr}, \tau_{cr}^*$	absolute [$M/L/T^2$] and nondimensionalised [-] critical bed shear-stress according to Shield diagram.
ω_y	vorticity, $\omega_y = \partial u / \partial z - \partial w / \partial x$ [$1/T$].

Subscript:

- ∞ approach flow.

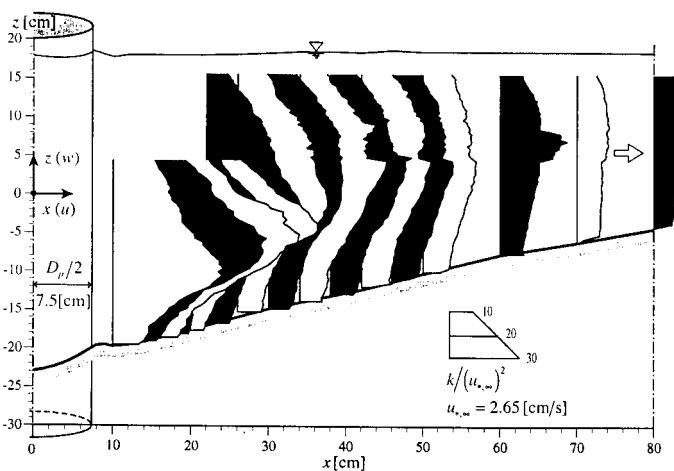


Fig. 12 Turbulent kinetic energy in the plane downstream of cylinder.

References

- AHMED, F., and RAJARATNAM, N. (1998). 'Flow around bridge piers.' *Am. Soc. Civ. Eng., J. Hydr. Engrg.*, 124(3), 288-300.
- DEY, S. (1997). 'Local scour at piers, part I: a review of developments of research.' *IRTCES, Int. J. Sediment Res.*, 12(2), 23-44.
- DEY, S., BOSE, S. K., and SASTRY, G. L. N. (1995). 'Clear water scour at circular piers: a model.' *Am. Soc. Civ. Eng., J. Hydr. Engrg.*, 121(12), 869-876.
- ETHERIDGE, D. W., and KEMP, P. H. (1978). 'Measurements of turbulent flow downstream of a rearward-facing step.' *J. Fluid Mech.*, 86(3), 545-566.
- GRAF, W. H., and ALTINAKAR, M. S. (1998). *Fluvial Hydraulics.*, J. Wiley & Sons, Ltd., Chichester, England.
- GRAF, W. H., and YULISTIYANTO, B. (1998). 'Experiments on flow around a cylinder; the velocity and vorticity fields.' *Int. Ass. Hydr. Res., J. Hydr. Res.*, 36(4), 637-653.
- HURTHUR, D., and LEMMIN, U. (2001). 'A correction method for turbulence measurements with a 3D acoustic Doppler velocity profiler.' *J. Atm. Ocean. Tech.*, 18(3), 446-458.
- ISTIARTO, I. (2001). 'Flow around a cylinder on a mobile channel bed.' *Ph.D. Thesis*, no. 2368, EPFL, Lausanne, Switzerland.
- KOBAYASHI, T., AIBARA, T., and HARADA, H. (1997). 'Vorticity distribution of horseshoe vortex on scoured bed.' *Proc. 27th Congress of the Int. Ass. Hydr. Res.*, San Francisco, California, Theme A, 202-207.
- LHERMITTE, R., and LEMMIN, U. (1994). 'Open-channel flow and turbulence measurement by high-resolution Doppler sonar.' *J. Atm. Ocean. Tech.*, 11, 1295-1308.
- MELVILLE, B. W. (1975). 'Local scour at bridge sites.' *Report No. 117*, University of Auckland, School of Engineering, New Zealand.
- MELVILLE, B. W., and RAUDKIVI, A. J. (1977). 'Flow characteristics in local scour at bridge piers.' *Am. Soc. Civ. Eng., J. Hydr. Engrg.*, 15(4), 373-380.
- NAKAGAWA, H., and NEZU, I. (1987). 'Experimental investigation on turbulent structure of backward-facing step flow in an open channel.' *Int. Ass. Hydr. Res., J. Hydr. Res.*, 25(12), 67-88.
- RAUDKIVI, A. J. (1991). 'Scour at Bridge Piers.', in *Scouring*, Ed. H. Breusers and A. J. Raudkivi, A.A. Balkema, Rotterdam, NL.
- RAUDKIVI, A. J. (1998). *Loose Boundary Hydraulics.*, A.A. Balkema, Rotterdam, NL.
- RICHARDSON, J. E., and PANCHANG, V. G. (1998). 'Three-dimensional simulation of scour-inducing flow at bridge piers.' *Am. Soc. Civ. Eng., J. Hydr. Engrg.*, 124(5), 530-540.
- SCHLICHTING, H. (1979). *Boundary Layer Theory.*, McGraw-Hill, New York, USA.
- SHEN, H. W. (1971). *River Mechanics, Vol. II, Chap. 23.*, H.W. Shen publ., Fort Collins, Colorado, USA.
- SHEN, H. W., OGAWA, Y., and KARAKI, S. S. (1963). 'Time variation of bed deformation near bridge piers.' *Proc. 10th Congress of the Int. Ass. Hydr. Res.*, London, Vol. 3.